Available online at www.sciencedirect.com
SCIENCE DIRECT®
Journal of Chromatography A, 1069 (2005) 119–126
JOURNAL OF CHROMATOGRAPHY A
www.elsevier.com/locate/chroma

Protein adsorption on the mesoporous molecular sieve silicate SBA-15: effects of pH and pore size

Amit Katiyar, Lei Ji, Panagiotis Smirniotis**, Neville G. Pinto*

Department of Chemical and Materials Engineering, University of Cincinnati, 401 Rhodes Hall, Cincinnati, OH 45221-0012, USA

Abstract

A mesoporous molecular sieve silicate, SBA-15, with three pore sizes (38.1 Å, 77.3 Å, and 240 Å) has been synthesized using a non-ionic, tri-block copolymer as a template in a sol–gel method. The effects of synthesis conditions on the pore size and pore-size distribution of this adsorbent have been described. The adsorption of proteins on these crystalline, ordered, materials has been studied. The kinetics of adsorption and equilibrium capacity have been probed with three proteins of different dimensions. The effects of electrostatic interactions and protein size are illustrated. It has been shown that SBA-15 materials can be tailored to show size selectivity for proteins, and very high capacities (450 mg/g) can be obtained. Furthermore, the rates of adsorption are shown to be dependent on the pore size, protein structure and solution pH.

Keywords: Size-selective; Adsorption; Proteins; Mesoporous; SBA-15

1. Introduction

Surfactant templated syntheses of silica supported mesoporous materials have played an important role in the field of materials during the last decade. The first member of this family, discovered by Mobil Oil, was MCM-41 [1,2]. The ordered hexagonal pore structure, high surface area, and inert framework of these materials have allowed use in a variety of applications including catalysis, chemical sensing, adsorption, and as hosts for large molecules. Protein separation and purification by chromatography is an important operation in the pharmaceutical industry, and the development of mesoporous materials as size-selective chromatographic supports holds promise for more efficient separations.

There are a few studies in the literature on the adsorption of proteins on siliceous molecular sieve [3–15]. Generally, it has been concluded that adsorption capacity is dependent on the pore size of the adsorbent relative to that of the protein, and a pore size slightly larger than the hydrodynamic radius is sufficient to obtain high capacities [9,10]. We have recently shown that an interpretation of the protein adsorption capacity must factor in the specific external surface area of these mesoporous materials [14,15]. The synthesis methods usually result in a morphology that has a significant specific external surface area which accounts for most of the capacity observed. Thus, without minimization of the external area relative to the pore area, the utility of these materials for size-selective separations is limited. Furthermore, it was observed that a pore size only slightly larger than the maximum dimension of the protein is inadequate, minimizing the utility of the MCM class of materials (pore diameter, 20–60 Å) for size-selective protein separations.

The limitations of the MCM materials have drawn attention to the larger-pore mesoporous silicates called SBA-15. This material was synthesized by Zhao et al. [16,17] using tri-block copolymers (P123, $PEO_{20}PPO_{70}PEO_{20}$) as a structure-directing agent. The formation of the mesostructure is based on the synthesis pathway (S^0H^+) (X^-I^+) under acidic condition (H^+X^-). The nonionic block copolymer (S^0) forms the organized structure due to self assembly of the template in aqueous solution. The process results in microphase separa-

* Corresponding author. Tel.: +1 513 556 2770; fax: +1 513 556 3930.
** Co-corresponding author.
E-mail addresses: panagiotis.smirniotis@uc.edu (P. Smirniotis), neville.pinto@uc.edu (N.G. Pinto).

0021-9673/$ – see front matter © 2004 Elsevier B.V. All rights reserved.
doi:10.1016/j.chroma.2004.10.077

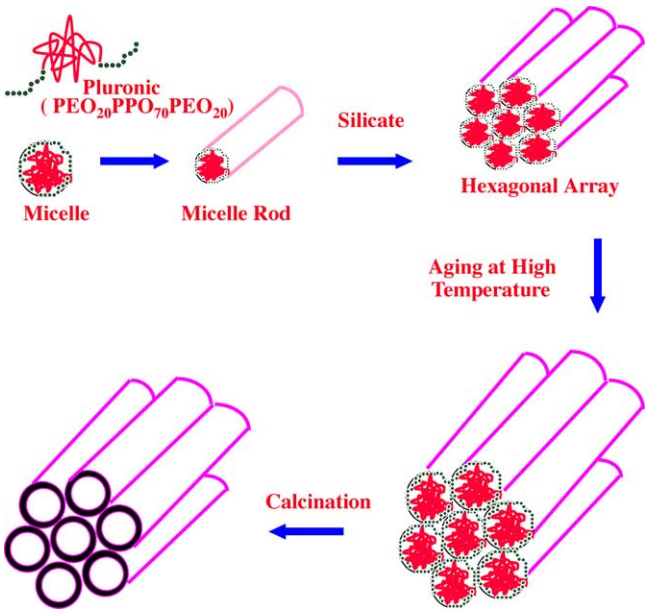

Fig. 1. Synthesis schematic for the formation of SBA-15.

tion and thus divides the space in hydrophilic and hydrophobic domains [18]. The micelle formed during the self assembly consists of a core of hydrophobic block PPO and a shell of hydrophilic block PEO. Under acidic conditions, the self assembly is followed by the hydrolysis and condensation of silica source (TEOS) which results in the formation of inorganic (I^+) network of silica. The synthesis route is shown in Fig. 1. These copolymers have the advantage that their ordering properties can be changed by altering the solvent composition and the copolymer architecture [16,17]. Furthermore, thicker pore walls are obtained in SBA-15, compared to MCM-41, which improves the hydrothermal stability of these materials. The pore-size range, sharp pore-size distribution, ordered pore structure, and the high specific pore area of SBA-15 are well suited for improving capabilities and efficiency in a variety of downstream bioseparation applications.

In this paper, the adsorption characteristics of bovine serum albumin (BSA), lysozyme (LYS), and myoglobin (MYO) on SBA-15 have been reported. The probe proteins were chosen for their molecular size, charge characteristics, and conformational stability [19–21]. For example, BSA has high conformational adaptability, while LYS is considered to be a "hard" protein. SBA-15 adsorbents with different pore sizes were synthesized, and the equilibrium and kinetic characteristics of the probe proteins on these materials have been studied.

2. Experimental

2.1. Materials

Lysozyme (L-6876), BSA (A-7030), myoglobin (M-0630), TRIZMA BASE (reagent grade: minimum, 99.9%) were purchased from Sigma (St. Louis, MO, USA) TEOS (tetraethyl orthosilicate) was purchased from Aldrich (Milwaukee, WI, USA). Hydrochloric acid, sodium acetate trihydrate, sodium azide (biotech research grade) and ammonium hydroxide (28%) are from Fisher Chemicals (Fair Lawn, NJ, USA). Glacial acetic acid was purchased from Pharmaco (Brookfield, CT, USA). 1,3,5-Trimethylbenzene and CTAB (cetylmethylammonium bromide) were obtained from Alfa Aesar (Ward Hill, MA, USA). Pluronics (P123, $PEO_{20}PPO_{70}PEO_{20}$) was a gift from BASF (Florham Park, NJ, USA).

Table 1
Summary of synthesis conditions for SBA-15

Material	Reaction temperature (°C)	Post-synthesis treatment (PST)		TMB/P123
		T (°C)	Time (h)	
SBA-15-1 (40 Å)	35	–	–	–
SBA-15-2 (80 Å)	35	100	48	–
SBA-15-3 (240 Å)	35	120	72	1:1

TMB: trimethylbenzene; P123: Pluronics ($PEO_{20}PP0_{70}PEO_{20}$).

2.2. Synthesis of adsorbents

SBA-15 was synthesized using Pluronics P123 ($PEO_{20}PPO_{70}PEO_{20}$) as a structure-directing agent and TEOS as the silica source. In a typical synthesis, 4 g of P123 dissolved in 104 g deionized water and 20 ml HCl (37%) was stirred for 30 min. TEOS (8.56 g) was added to the solution, which was vigorously stirred for 24 h at 35 °C [22], followed by post-synthesis treatment at different temperatures for 48–72 h, depending upon the targeted pore size. TMB was used, in an appropriate ratio with the surfactant, as a swelling agent for increasing the pore size. The synthesis conditions are summarized in Table 1.

The solid products were filtered and then washed with DI water repeatedly. The solid products were dried at room temperature and calcined in ambient air from room temperature to 550 °C, with a heating rate of 1 °C/min. At the end, the heating ramp, the temperature was held constant at 550 °C for 6 h. The cooling rate was 5 °C/min.

2.3. Characterization

X-ray diffraction (XRD) was used to identify the crystal phases of the SBA-15 materials. For the smallest pore-size material SBA-15-1 (38 Å diameter), the experiments were performed on a Siemens D500 power X-ray diffractometer equipped with a Cu Kα radiation source (wavelength, 1.5406 Å) run at 40 kV, 30 mA. XRD patterns were obtained from 1° to 7° of 2θ, with a step size of 0.01° and the time step of 1 s.

Small angle X-ray scattering (SAXS) was used for the determination of crystalline structure in the larger pore SBA-15 (77 Å and 240 Å). The experiments were performed on the University of Minnesota two-dimensional small angle

X-ray line. The SAXS line has copper radiation, frank mirrors, a variable-temperature evacuated sample chamber and a multiwire area detector (GADDS). The powder samples were placed in 1.0 mm diameter special glass capillaries from Charles Supper. One of the variables in SAXS is the sample-to-detector distance. Varying the sample-to-detector distance changes the range of *d*-spacing that the detector can collect. A shorter distance will show smaller structures and will have a larger angular range, whereas a longer distance will show larger structures and have better resolution. Three detector distances were used due to the wide variety of pore sizes: 38 cm (126–12 Å), 100 cm (360–35 Å) and 230 cm (550–90 Å). Sample collection time varied from 200 s to 300 s per sample.

Nitrogen adsorption–desorption measurements were performed at 77 K on a Micromeritics ASAP 2010 volumetric adsorption analyzer. SBA-15 (50 mg) was degassed at 573 K for 4 h in the degassing port of the adsorption apparatus. The surface-area measurement is based on the BET method, and the pore-size distribution is based on the BJH method.

SEM was performed on Hitachi S-4000 scanning electron microscope. The samples were prepared by placing SBA-15 powder on double-sided carbon adhesive tape mounted on the sample holder.

2.4. Protein adsorption

Batch adsorption experiments were carried out by contacting 50 mg of SBA-15 with protein solution for different periods of time. The adsorbent and solution were vigorously shaken in a G24 Environmental Incubator Shaker (New Brunswick Co.) at 180 rpm and 25 °C. The equilibrated samples were centrifuged for 10 min at 10,000 rpm. The supernatant was diluted in a buffer and then filtered through a 0.2 μm HT Tuffryn low protein binding membrane filters. The protein concentration in the supernatant was analyzed on a UV spectrophotometer (Spectronic 1001, Milton Roy) at 280 nm. A mass balance was applied to calculate the protein adsorbed on the SBA-15. The experiments were carried out at selected solution pH values with 50 mM of appropriate buffer. The kinetic experiments were performed using a starting protein solution concentration of 10 mg/ml. A blank run was performed with each experiment for good control on experimental conditions.

3. Results and discussion

3.1. Characterization of SBA-15

The XRD spectrum for the smallest pore SBA-15 (SBA-15-1) obtained on the Siemens D500 is shown in Fig. 2a. Two peaks are observed between 2θ ranging from 1.5° to 7°, as expected. These correspond to the d_{110} and d_{200} spacings, respectively, and indicate long-range order in the material. The peak for d_{100} spacing for SBA-15-1 (38.1 Å) is in the small-angle region, anticipated below 1.5°, and is, therefore, not observed. However, from the d_{110} and d_{200} peaks and data already available in the literature [23], the crystallinity and pore size of the material can be accessed. The pore diameter using d_{200} spacing was found to be 51 Å, while the KJS method [24] estimates the pore diameter as 52 Å. These are higher than the value estimated from the BJH method (38.1 Å), which is consistent with reports in the literature that the BJH method underestimates the pore diameter [25].

Small angle X-ray spectra for the larger pore SBA-15 materials are shown in Fig. 2b and c. These show a sharp peak with d_{100} spacing of 97 Å (SBA-15-2) and 242 Å (SBA-15-3), respectively. In both cases, two weak, well resolved peaks with d_{110} and d_{200} spacing are also observed. The presence of three peaks confirms the highly crystalline structure of the synthesized materials. The corresponding unit cell parameters calculated using $a_0 = 2d_{100}/\sqrt{3}$ are listed in Table 2. The large pore-wall thickness (W) indicates that the SBA-15 materials have good stability.

The BET surface area for all three SBA-15 materials is high (Table 2). The external surface area was calculated using the α-plot method [26], to ensure that it is small compared to the pore area. The external surface area for SBA-15-1 is 22 m^2/g, while for SBA-15-2 and SBA-15-3 it is less then 15 m^2/g. It is noted that the BET surface area for SBA-15-2 is higher than for the other two materials. This is a result of the synthesis conditions used (Table 1), particularly the combination of the selected post-synthesis treatment (PST) temperature and the absence of a swelling agent; the selected conditions appear to be optimum for maximizing the BET surface area.

The pore-size distributions in Fig. 3 illustrate that sharp distributions can be obtained, relative to conventional, non-crystalline silica supports [27]. The synthesis procedures can be tuned to sharpen these distributions further. For example, PST can be used to minimize microporosity. The synthesis of SBA-15-1 was performed without PST, and this material has the largest microporous volume. PST decreases the microporosity by reducing penetration of the silica walls by the hydrophilic PEO blocks [28]. Microporosity in SBA-15-2 was reduced with PST performed at 100 °C for 48 h, and microporosity in SBA-15-3 was virtually eliminated with PST at 120 °C for 72 h.

The BJH pore-size is summarized in Table 2. It is observed that the selection of the PST and swelling agent can be combined to control the pore size of the materials, which is desired in developing size-selective chromatographic media. The morphology of these materials is also important for commercialization for protein separations. SBA-15 particles synthesized with uncontrolled morphology showed a fiber-like structure with length >30 μm (Fig. 4a), which consist of small agglomerated rod shaped primary particles (Fig. 4b). Since the purpose of this study was to investigate the potential for size-selectivity with SBA-15, the control of particle morphology is not addressed, but is the subject of a separate study to develop spherical particles for chromatographic use.

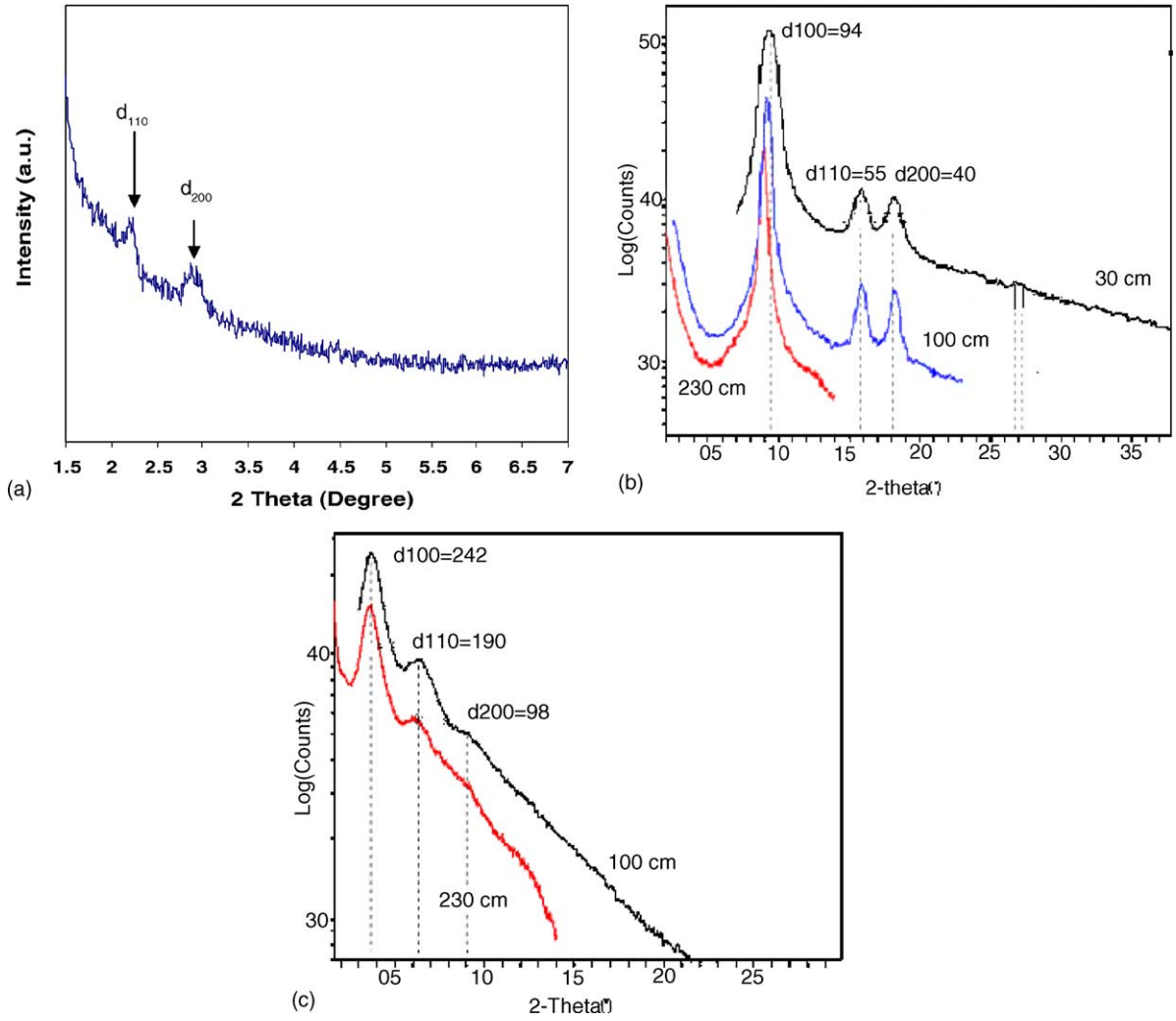

Fig. 2. (a) XRD of SBA-15-1; (b) SAXS of SBA-15-2; (c) SAXS of SBA-15-3.

Table 2
Properties of SBA-15 materials used for protein adsorption studies

Material	D_{BJH} (Å)	d_{100} (Å)	a_0 (Å)	W (Å)	BET surface area (m^2/g)	Pore volume (cm^3/g)
SBA-15-1	38.1	–	48.84	10.74	613	0.47
SBA-15-2	77.3	97	112.05	34.75	912	1.16
SBA-15-3	240	242	277.95	37.95	570	2.28

D_{BJH}: BJH pore diameter; d_{100}: XRD (1 0 0) interplaner spacing; a_0: unit cell parameter; W: pore-wall thickness.

3.2. Protein adsorption

The kinetics of lysozyme (LYS) adsorption on SBA-15-2 at pH 5 and 8 are shown in Fig. 5. Since LYS has dimensions of 30 Å × 30 Å × 45 Å [20], it is expected that the protein has access to the pore area of SBA-15-2 (77 Å). The high equilibrium capacity (>200 mg/gm) indicates that this is the case, since the specific external surface area for SBA-15-2 is small, <15 m^2/g. Furthermore, it is noted (Fig. 6) that the equilibrium adsorption capacity and the protein uptake rate of the largest pore material SBA-15-3 (240 Å) is similar to that for SBA-15-2 at the same solution conditions (pH 5). Since the pore size of SBA-15-3 is much larger than the protein, this leads to the conclusion that the accessible surface area for protein adsorption is similar for the two materials, and is in the pores. Furthermore, it also

Table 3
Physical properties of probe proteins

Protein	Molecular mass	Isoelectric point	Dimension	Reference
BSA	69000	4.9	40 Å × 40 Å × 140 Å	[19]
Lysozyme	14400	11	30 Å × 30 Å × 45 Å	[20]
Myoglobin	17600	7.0–7.2	25 Å × 35 Å × 45 Å	[21]

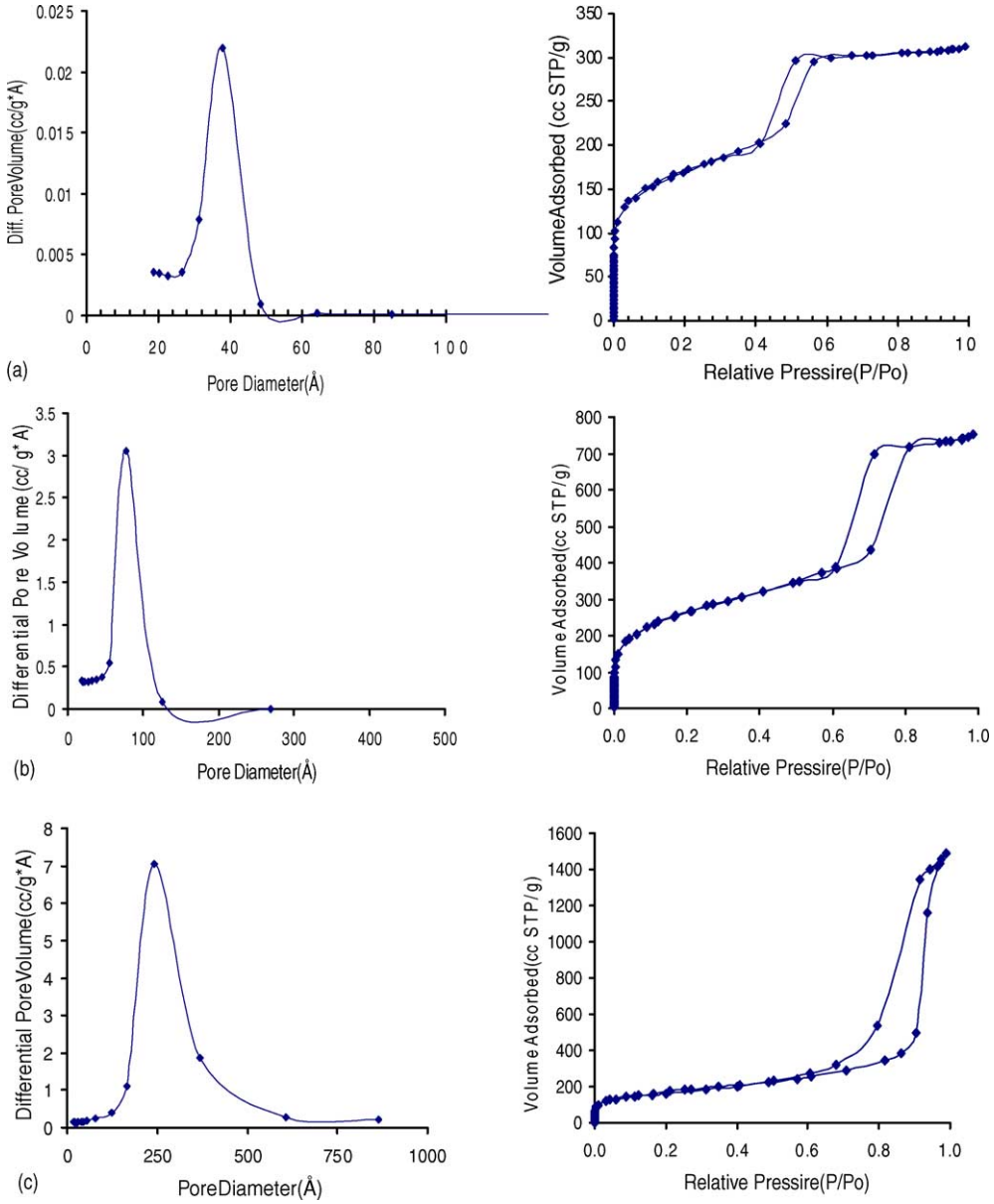

Fig. 3. BJH pore-size distribution and nitrogen adsorption–desorption isotherms for (a) SBA-15-1; (b) SBA-15-2; (c) SBA-15-3.

indicates that the higher N_2 BET surface area (Table 2) for SBA-15-2 is due to small mesopores or micropores (as seen in Fig. 3), which are not accessible for protein adsorption.

The rate curves in Fig. 5 clearly show an effect of pH on protein uptake. At both pH conditions, the adsorbent has a strong affinity for the protein, and the rate curves are essentially identical for the first 6 h. However, at pH 5, the equilibrium capacity is attained within 6 h, while at pH 8, it takes over 120 h to attain a higher equilibrium capacity. The difference can be explained on the basis of differences in electrostatic interactions between the protein and adsorbent, and differences in repulsive interactions between adsorbed proteins.

At both pH conditions, the SBA-15 is negatively charged and LYS is positively charged. Initial adsorption is driven by attraction between the protein and the adsorbent surface. As surface coverage increases, electrostatic repulsion between adsorbed proteins becomes more significant. Iler [27] has shown that the charge density of negatively charged silica is almost constant between pH 4 and 8, while Tanford and Roxby [29] found that net positive charge on lysozyme increases from 8 at pH 8 to 10 at pH 4. Thus, repulsive interactions between adsorbed proteins are expected to be stronger at pH 5 compared to pH 8, and more significant at the lower pH relative to the primary adsorbent-protein interaction. Su et al. [30] reached a similar conclusion, showing that that pH dependence of protein adsorption is dominated

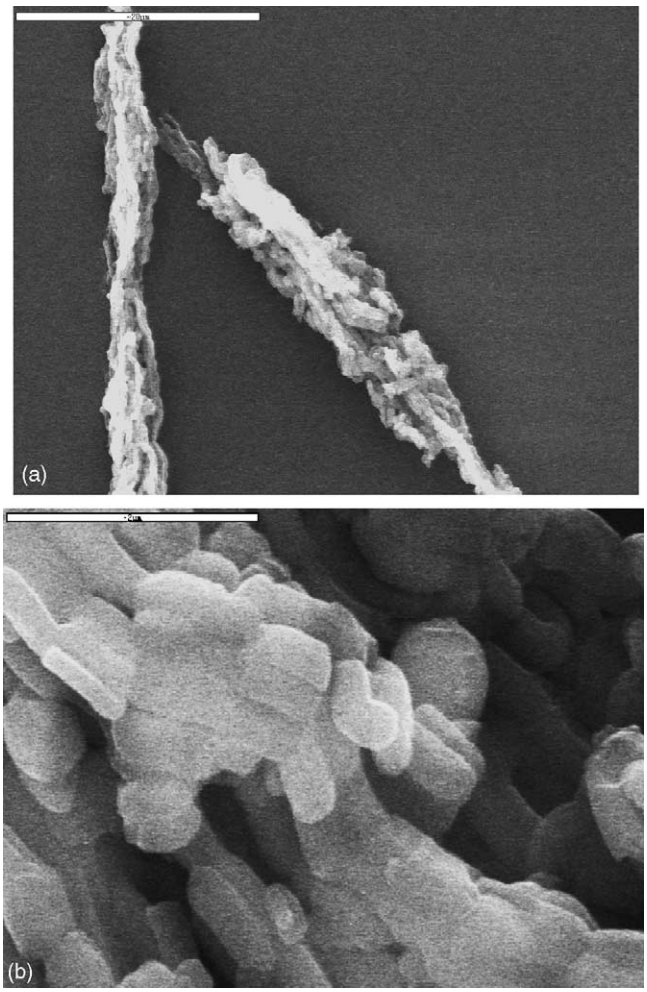

Fig. 4. (a) Fibrous structure of SBA-15 particles; (b) rod-like primary particles aggregate to form micron-sized fibers.

by protein–protein interactions rather than protein-surface interactions. They reported that LYS occupies 14 nm^2 at pH 8 and 26.6 nm^2 at pH 5, and there is no change observed in this area with time. The larger area occupied at the lower pH

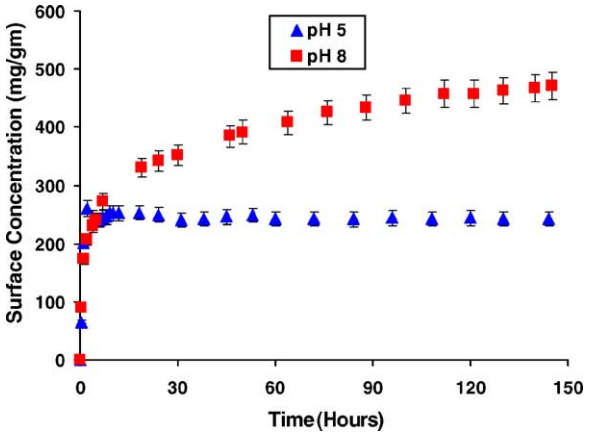

Fig. 5. Rate of adsorption of lysozyme at pH 5 and pH 8 on SBA-15-2.

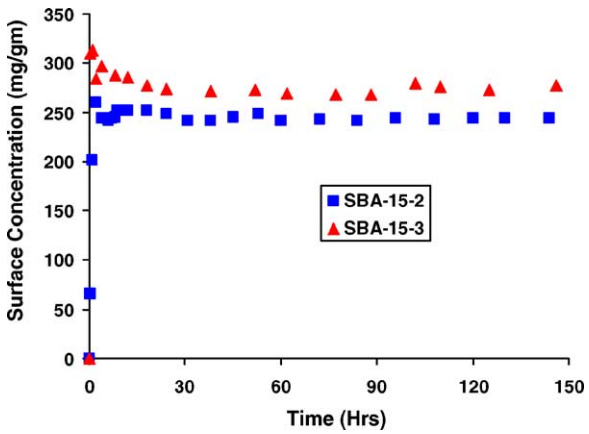

Fig. 6. Effect of pore size on rate of adsorption of lysozyme at pH 5.

is a consequence of the stronger protein–protein repulsive interactions.

Since the isoelectric point of LYS (pI = 11) is above the stability limit of SBA-15, the effect of a change in net charge on the protein adsorption cannot be studied with this protein. Myoglobin (MYO), which has a pI = 7–7.2, was used for this purpose (Table 3). Shown in Fig. 7 is the rate of adsorption of MYO on SBA-15-2 at three solution pH conditions: 5, 7 and 8.5. These data clearly show the importance of electrostatic interactions. At a pH of 8.5 the equilibrium capacity is very low (≈25 mg/g) because both MYO and SBA-15 have a net negative charge. For pH ≤ pI, the equilibrium capacity is very high: ≈275 mg/g at pH 5, and ≈250 mg/g at pH 7.2. The latter pH corresponds to the pI of the protein. Kondo and Mihara [31] have reported similar behavior for the adsorption of MYO on ultrafine silica particles. They attributed the high capacity at pH < pI to monolayer coverage with a high packing density.

The dependence of the protein capacity of SBA-15 on the pore size was studied by measuring the adsorption isotherms of LYS and BSA. These proteins were selected to determine if SBA-15 can be tailored to be size selective for chromatographic applications. The largest dimension of BSA is 140 Å;

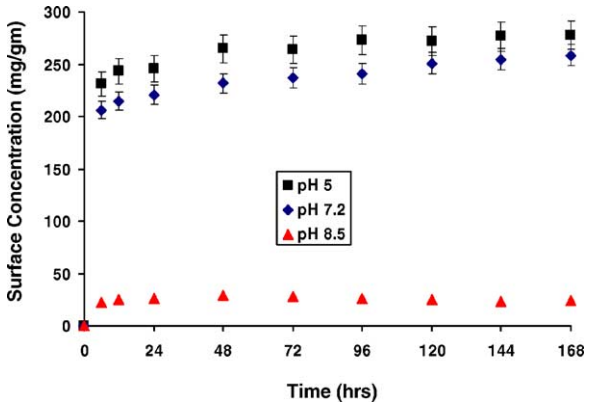

Fig. 7. Rate of adsorption of myoglobin on SBA-15-2 at different pH conditions.

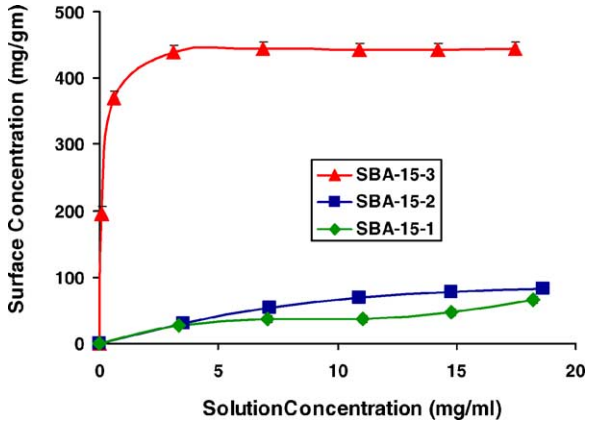

Fig. 8. Effect of pore size of SBA-15 on equilibrium adsorption isotherms for BSA at pH 5.

thus, this protein should effectively be excluded from the pore area of SBA-15-1 (38 Å) and SBA-15-2 (77 Å). Since the largest dimension of LYS is 45 Å, this protein should show good capacity on SBA-15-2 and SBA-15-3 (240 Å), and a low capacity on SBA-15-1. Adsorption isotherms were measured at pH 5 for both proteins. At this condition, the equilibrium distribution for LYS was attained within 24 h and for BSA within 146 h.

Shown in Figs. 8 and 9, respectively, are the adsorption isotherms for BSA and LYS. In Fig. 8, it can be seen that SBA-15-1 and SBA-15-2 have a low capacity for BSA, indicating that the pore surface area is, in general, not accessible. In contrast, the large-pore SBA-15-3 material has a very high capacity (>450 mg/g) for the protein. This high capacity is attributed to two factors: the very high specific surface area available in the adsorbent, and the minimization of repulsive electrostatic interactions between adsorbed proteins due to adsorption close to the protein p*I*.

LYS adsorption isotherms confirm the capability for achieving size selectivity in SBA-15 materials. In Fig. 9, SBA-15-2 and SBA-15-3 show similar capacities for LYS, while the small-pore SBA-15 has a very small capacity for

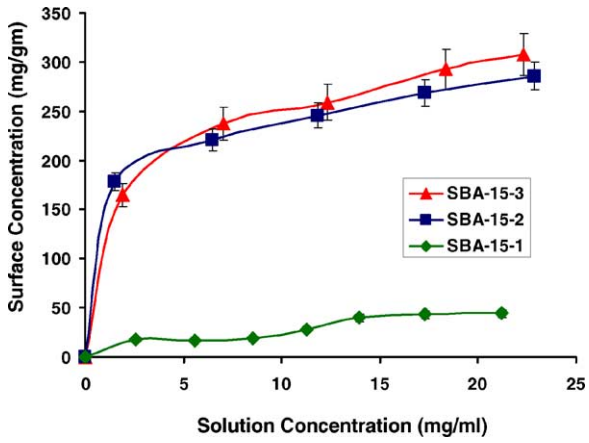

Fig. 9. Effect of pore size of SBA-15 on equilibrium adsorption isotherms for lysozyme at pH 5.

this protein, most of which is probably due to adsorption on the external surface of the particles. It is noted that the capacity SBA-15-3 for LYS is substantially lower than for BSA because at pH 5 LYS has a net charge, and repulsive interactions between adsorbed proteins, as described earlier, limit capacity.

4. Conclusions

It has been shown that siliceous SBA-15 adsorbents can have a very high affinity and capacity for proteins. The adsorption capacity and rate of adsorption is dependent on the solution pH, due to the strong influence of electrostatic interactions, and protein and pore size. Most significantly, for chromatographic applications, SBA-15 adsorbents can be tailored to be size selective for proteins. Additionally, because of the ordered nature of these materials, very high specific surface areas can be obtained, and these can result in very high protein adsorption capacities.

Acknowledgement

The authors gratefully acknowledge financial from the National Science Foundation under Grant No. CTS-0241159.

References

[1] J.S. Beck, J.C. Vartuli, W.J. Roth, M.E. Leonowicz, C.T. Kresge, K.D. Schmitt, C.T. Chu, D.H. Olson, E.W. Sheppard, S.B. McCullen, J.B. Huggins, J.L. Schelenker, J. Am. Chem. Soc. 114 (1992) 10834.
[2] C.T. Kresge, M.E. Leonowicz, W.J. Roth, J.C. Vartuli, J.S. Beck, Nature 359 (1992) 710.
[3] J.F. Diaz, K.F. Balkus Jr., J. Mol. Catal. B: Enzym. 2 (1996) 115.
[4] J. He, X. Li, D.G. Evans, X. Duan, C. Li, J. Mol. Catal. B: Enzym. 11 (2000) 45.
[5] J.M. Kisler, G.M. Stevens, A.J. O'Connor, Mater. Phys. Mech. 4 (2001) 89.
[6] H. Takahashi, B. Li, T. Sasaki, C. Miyazaki, T. Kajino, S. Inagaki, Microporous Mesoporous Mater. 44–45 (2001) 755.
[7] H.H.P. Yiu, P.A. Wright, N.P. Botting, J. Mol. Catal. B: Enzym. 15 (2001) 81.
[8] H.H.P. Yiu, P.A. Wright, N.P. Botting, Microporous Mesoporous Mater. 44–45 (2001) 763.
[9] J. Deere, E. Magner, J.G. Wall, B.K. Hodnett, Chem. Commun. 2001 (2001) 465.
[10] H.H.P. Yiu, C.H. Botting, N.P. Botting, P.A. Wright, Phys. Chem. Chem. Phys. 3 (2001) 2983.
[11] J. Deere, E. Magner, J.G. Wall, B.K. Hodnett, J. Phys. Chem. B 106 (2002) 7430.
[12] J. Zhao, F. Gao, Y. Fu, W. Jin, P. Yang, D. Zhao, Chem. Commun. 2002 (2002) 752.
[13] A. Vinu, V. Murugesan, M. Hartmann, J. Phys. Chem. B 108 (2004) 7323.
[14] A. Katiyar, L. Ji, P. Smirniotis, N. Pinto, Microporous Mesoporous Mater., in press.
[15] L. Ji, A. Katiyar, N. Pinto, P. Smirniotis, Microporous Mesoporous Mater. 75 (2004) 221.

[16] D. Zhao, J. Feng, Q. Huo, N. Melosh, G.H. Fredrickson, B.F. Chmelka, G.D. Stucky, Science 279 (1998) 548.
[17] D. Zhao, Q. Huo, J. Feng, B.F. Chmelka, G.D. Stucky, J. Am. Chem. Soc. 120 (1998) 6024.
[18] G.J.A.A. Solerillia, E.L. Crepaldi, D. Grosso, C. Sanchez, Curr. Opin. Colloid Interface Sci. 8 (2003) 109.
[19] Y.I. Tarasevich, Theor. Exp. Chem. 37 (2001) 98.
[20] H. Shirihama, J. Lyklema, W.J. Norde, J. Colloid Interface Sci. 139 (1990) 177.
[21] M.A. Bos, Z. Shervani, A.C.I. Anusiem, M. Giesbers, W. Norde, M. Kleijn, Colloids Surf. B: Biointerfaces 3 (1994) 91.
[22] Y. Wang, M. Noguchi, Y. Takahashi, Y. Ohtsuka, Catal. Today 68 (2001) 3.
[23] M. Kruk, M. Jaroniec, C.H. Ko, R. Ryoo, Chem. Mater. 12 (2000) 1961.
[24] M. Kruk, M. Jaroniec, A. Sayari, Langmuir 13 (1997) 6267.
[25] P.I. Ravikovitch, S.C.O. Domhnaill, A.V. Neimark, F. Schueth, K.K. Unger, Langmuir 11 (1995) 4765.
[26] A. Sayari, P. Liu, M. Kruk, M. Jaroniec, Chem. Mater. 9 (1997) 2499.
[27] R.K. Iler, The Chemistry of Silica, Wiley, New York, 1978.
[28] A. Galarneau, H. Cambon, F.D. Renzo, R. Ryoo, M. Choi, F. Fajula, N. J. Chem. 27 (2003) 73.
[29] C. Tanford, R. Roxby, Biochemistry 11 (1972) 2192.
[30] T.J. Su, J.R. Lu, R.K. Thomas, Z.F. Cui, J. Penfold, Langmuir 14 (1998) 438.
[31] A. Kondo, J. Mihara, J. Colloid Interface Sci. 177 (1996) 214.